Estimation of Design Parameters and Performance for a State-of-the-Art Turbofan

Proceedings of the ASME Turbo Expo 2021
Turbomachinery Technical Conference and Exposition
GT2021
June 7-11, 2021, Virtual, Online

GT2021-59489

ESTIMATION OF DESIGN PARAMETERS AND PERFORMANCE FOR A STATE-OF-THE-ART TURBOFAN

Oliver Sjögren[1], Carlos Xisto[1], Tomas Grönstedt[1]

[1]Chalmers University of Technology, Göteborg, Sweden

ABSTRACT

The aim of this study is to explore the possibility of matching a cycle performance model to public data on a state-of-the-art commercial aircraft engine (GEnx-1B). The study is focused on obtaining valuable information on figure of merits for the technology level of the low-pressure system and associated uncertainties. It is therefore directed more specifically towards the fan and low-pressure turbine efficiencies, the Mach number at the fan-face, the distribution of power between the core and the bypass stream as well as the fan pressure ratio. Available cycle performance data have been extracted from the engine emission databank provided by the International Civil Aviation Organization (ICAO), type certificate datasheets from the European Union Aviation Safety Agency (EASA) and the Federal Aviation Administration (FAA), as well as publicly available data from engine manufacturer. Uncertainties in the available source data are estimated and randomly sampled to generate inputs for a model matching procedure. The results show that fuel performance can be estimated with some degree of confidence. However, the study also indicates that a high degree of uncertainty is expected in the prediction of key low-pressure system performance metrics, when relying solely on publicly available data. This outcome highlights the importance of statistic-based methods as a support tool for the inverse design procedures. It also provides a better understanding on the limitations of conventional thermodynamic matching procedures, and the need to complement with methods that take into account conceptual design, cost and fuel burn.

Keywords: performance modelling, propulsion, latin hyper-cube sampling

NOMENCLATURE

C_V	Nozzle velocity coefficient
F_N	Net thrust
$\hat{F}_N$	Specific net thrust
h	Specific stagnation enthalpy
M	Mach number
n	Sample point
N	Sample size
P	Stagnation pressure
PR_n	Pressure split exponent
r_m	Blade mean radius
U	Tangential blade speed
V	Flow velocity
W	Mass flow

Greek

δ_η	Efficiency factor
ζ	Ideal exhaust jet velocity ratio
η	Efficiency
$\overline{\psi}$	Average stage loading coefficient
μ	Statistical mean
σ	Standard deviation
Π	Pressure ratio
Ω	Shaft rotational speed

Subscripts

B	Bleed
R	Referred (Corrected)
f	Fuel
I	Ideal
P	Polytropic

Superscripts

$( )^*$	Normalized quantity

Abbreviations

BPR	Bypass ratio
EASA	European Aviation Safety Agency
EDB	Engine emission databank
EIS	Entry into service
FAA	Federal Aviation Agency
FPR	Fan pressure ratio
HPC	High pressure compressor

HPT	High pressure turbine
HPX	High pressure system power off-take
ICAO	International Civil Aviation Org.
ISA	International Standard Atmosphere
LPC	Low pressure compressor
LPT	Low pressure turbine
MCR	Max cruise
TO	Take-off
TOC	Top-of-climb
SLS	Sea level static

1. INTRODUCTION

When modelling future turbofan engines, critical design parameters such as fan pressure ratio, bypass ratio, and overall pressure ratio will have a major impact on the predicted performance. Most often these parameters are obtained by means of optimization. Because of the multidisciplinary character of these types of problems, the resulting design will depend on the scope of the study as well as the objectives of the optimization. A too narrow scope could lead to suboptimal solutions while conflicting objectives might result in ambiguity. Uncertainties in these approaches brings about the need to verify the methods against actual data on state-of-the-art engines in use today. Unfortunately, due to the proprietary nature of such data, one will be forced to model these engines as well. Matching a cycle performance model against data from rig tests or under-the-wing operation on existing engines is a common practice in the industry. Performance data from these models are a vital tool for engine health diagnostics [1]. If one would be able to match engine performance models against publicly available data on state-of-the-art engines with enough precision, this would - in the author's opinion - be a valuable complement to studies of a more exploratory nature predicting future technology trends [2].

Engine design will undoubtedly introduce uncertainties in the input data due to manufacturing tolerances, measurement accuracy, technology projections etc. The same rationale applies to the inverse engine design matching procedure; emissions data in a test rig are collected with a certain level of accuracy; component efficiencies are usually correlated with public data; cooling flow is normally estimated with analytical models that do not fully appreciate the complexity of the turbine cooling heat transfer process, etc. All the aforementioned issues will further increase the uncertainty while predicting the performance during engine design or engine matching procedures. The effects of uncertainty in component efficiencies, and its importance on the overall performance of aircraft engines in the preliminary design phase, have been investigated by Mavris et. al. [3, 4]. Kyprianidis et. al. [5], investigated the impact of uncertainties in the thermo-fluid properties modelling and its impact on the propulsion system performance. Their study points to the increasing importance of a careful balance between accuracy and computational time as the technology level is further pushed to its limits.

The present paper is focused on estimating the performance metrics, and their interrelationship, of today's civil turbofans, such as fan pressure ratio, fan-face Mach number and high-low pressure system power split. This is achieved by applying an inverse model-matching approach on the GEnx-1B engine. This approach makes use of efficiency correlations for turbomachinery components together with publicly available data obtained from the aircraft engine emission databank, type certificate data sheets and data publicly provided by the engine manufacturer. The study is supported by random sampling of the inputs where uncertainties are estimated for the publicly available data and the correlations. The outcome is an estimation of the design parameters and performance metrics of interest as well as their influence on each other in terms of statistical measures for this particular inverse design problem. To the authors' knowledge, it is the first time that such a study is carried out. This work will thus aim at quantifying the limitations of engine cycle matching using publicly available data sources on contemporary engines.

2. METHODOLOGY

In traditional performance modelling, the process starts with the definition of the thermodynamic point, followed by the calculation of off-design performance for a specified set of operating conditions. However, public data is normally available for different operating points and cannot be used to single out the design condition of the engine. The approach used in this study is therefore to iteratively find the thermodynamic cycle design, based on known performance data in both on-design and off-design points. The Chalmers in-house gas turbine simulations tool GESTPAN [6 – 11] is used for the performance evaluation in design and subsequent off-design points. To ensure that the performance model fulfills the constraints set by the known data, an external solver is wrapped around GESTPAN. The solver capabilities available in the open source framework OpenMDAO are used for this purpose [12]. The external solver handles the performance code as a "black-box", where appropriate independent-dependent variable pairs are defined in terms of the available inputs and outputs for the GESTPAN model. The model responses are evaluated using finite difference and the Jacobian of the system is updated with the Broyden method. Details about the model and the external solver setup are described in section 2.1 and 2.2.

Due to measurement uncertainties and scatter in the source data, uncertainties in the output will be expected as well. To account for this, the uncertainties in the known data have been estimated in terms of probability distributions. *N* Sets of input data are then generated by means of random sampling, after which the model matching step described above is executed for each sample point *n*. A more detailed description of the sampling technique and the setup is provided in section 2.3. In Figure 1, an overview of the steps in the procedure are illustrated in a flow-chart.

2.1 Engine architecture and performance modelling

The engines of the GEnx family are two-spool, direct drive, separate flow turbofans intended for medium- to long-range transport airliners. Out of the two available models: 1B and 2B

the former will be studied here. The engine model comes in different take-off thrust ratings ranging from about 54,000 to 76,000 lbf at sea level static condition (SLS). Only the higher rated engines will be targeted in this study, more specifically the GEnx-1B74/75/P2 that serves as the propulsion system for the Boeing 787-9 airplanes [20].

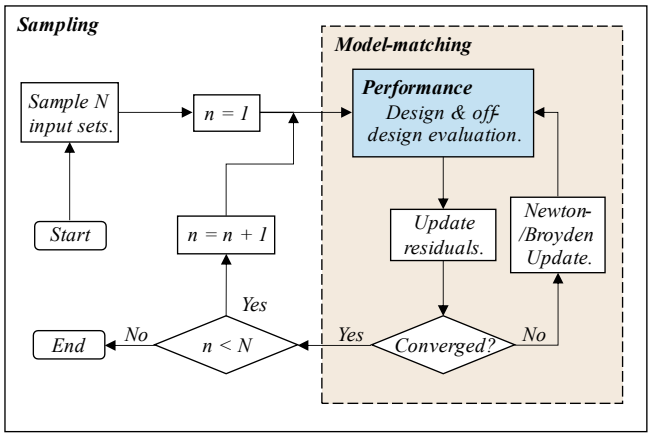

Figure 1: Flow-chart of the model matching procedure with the random sampling of inputs. Each sample point *n* will result in a performance cycle fulfilling the requirements specified by the current input data set.

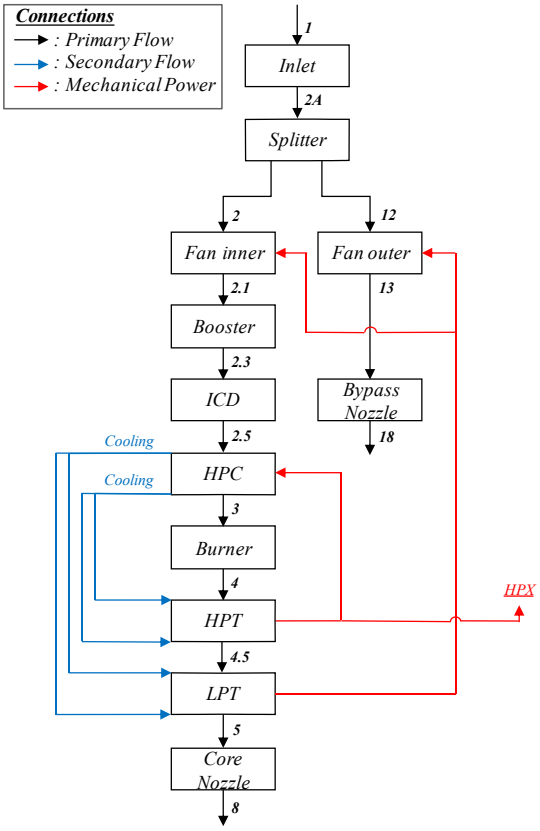

Figure 2: Schematic of the GEnx-1B performance model in GESTPAN including station numbering.

The GESTPAN performance models are created by defining connections for pre-defined engine component modules. A basic schematic of the GESTPAN representation of the GEnx-1B engine with station numbering is shown in Figure 2. Since the Boeing's 787-models have an independent system providing pressurized air to the cabin, there is no need for customer bleed from the HPC. Instead, the cabin air compression is accomplished with power off-take from the high-pressure spools.

2.1.1 Component efficiencies

Compressor and turbine efficiencies in design, are determined with trend curves based on correlations from a statistical study done by Grieb in 2004 [13]. The data for the civil engines in Grieb's study are provided for max cruise (MCR) and for that reason the same operating point is chosen for design in the current study. This entails an altitude and Mach number of 35000ft and 0.85 respectively. The thrust rating is defined by prescribing a ratio to the thrust in top-of-climb (TOC) in accordance with ref. [13].

The efficiency correlations from Grieb's study are based on the assumption that the polytropic efficiency can be broken down into a normalized polytropic efficiency (η_P^*) depending on the average stage loading only ($\overline{\psi}$), and linearly independent terms that accounts for the effects of entry into service (EIS), Reynolds number index (RNI), and inlet standard day corrected mass flow (W_R), respectively. This relationship is expressed in Eqn. (1),

$$\eta_P = \eta_P^* + \Delta\eta_{\text{EIS}} + \Delta\eta_{\text{RNI}} + \Delta\eta_{WR}, \tag{1}$$

where η_P^* – normalized with respect to EIS = 1995, RNI = 1.0 and W_R = 70kg/s – is given by a relation:

$$\eta_P^* = f(\overline{\psi}). \tag{2}$$

Each expression on the left-hand side of Eqn. (1) are provided by Grieb in terms of raw data. In the work by Samuelsson et. al. [14] this data was correlated into trend curves and implemented into a conceptual design optimization framework for civil turbofan engines. The expression in Eqn. (2) have for the purpose of this study been obtained by adapting trend lines in the same manner, but with an additional free parameter to account for uncertainties due to the scatter of the source data. How the uncertainties are quantified and implemented into the framework is discussed in more detail in section 2.3.1. It should be noted that for fan components, the normalized efficiency is correlated against the pressure ratio (FPR) instead of $\overline{\psi}$. The expressions for the individual effects given by the $\Delta\eta$-terms are implemented in the same way as in [14]. With regards to cooled turbines, the normalized polytropic efficiency is further divided into one without the influence from cooling flow and a component accounting for the effects of cooling accordingly:

$$\eta_P^* = \eta_{P,uncooled}^* + \Delta\eta_{cooled}. \tag{3}$$

In summary, Eqns. (1-3) will provide component polytropic efficiencies for given inputs of $\overline{\psi}$, EIS, RNI, W_R, and cooling flow.

2.1.2 Average stage loading

To evaluate the efficiency of the booster, the HPC, the HPT and the LPT according to the method described in section 2.2.1, the average stage loading – as defined in Eqn. (4) – has to be calculated in the design point for each component.

$$\overline{\psi} = \frac{2\Delta h}{\sum U^2} \tag{4}$$

The difference in specific stagnation enthalpy over the entire component – denoted Δh in Eqn. (4) – is obtained as an output from the performance modelling. The variable U represents the tangential blade speed for a given stage and the summation is carried out over all stages in the component. The tangential rotor-velocity for a given stage is evaluated at the mean radius of the rotor blade, denoted r_m. The mean radius for each stage and component have been estimated based on available engine diagrams. The rotational speed of the low and the high pressure spool, (Ω_L and Ω_H) at 100% power setting for a standard day take-off at sea-level-static operating condition ($\mathrm{TO_{ISA}}$), are provided in [15] and reproduced in Appendix A. With the ratio between the mechanical spool speed at MCR to $\mathrm{TO_{ISA}}$ provided as an output from the performance modelling, the absolute rotor-speed of the component at MCR can be calculated. The average stage loading for a given component at MCR, is then computed accordingly:

$$\overline{\psi}_{MCR} = \frac{2\Delta h_{MCR}}{(\pi\Omega_{MCR})^2 \sum r_m^2}. \tag{5}$$

2.1.3 Turbine cooling

Specific details on the advanced technologies making efficient turbine cooling possible are well kept company secrets. Hence finding open sources with reliable data on cooling flow ratios for a particular engine model is most often a difficult, if not impossible task. Nevertheless, for existing engines 20-30% of core inlet flow used for cooling purposes, have been indicated [16]. This intends the total flow extracted from the HPC – including non-chargeable flow – for cooling of both the HPT and the LPT. In the present study, nominal values of 22% is assumed to be used to cool the two-stage HPT turbine and 5% to cool the two first stages of the LPT turbine. In every stage, 50 percent of the cooling flow is assumed to be used for stator vane cooling for both the HPT and the LPT.

2.1.4 Power off-take

The customer power extraction from the high-pressure rotor (HPX) is estimated based on certified values for maximum power extraction and/or torque for aircraft electrical and hydraulic generation. Data on this is available in the type certificate datasheets [17, 15]. Maximal allowed power extracted at 100% rotational speed is 517.5 kW. In the present study a 35% margin towards this value is assumed, yielding about 330 kW.

2.1.5 Fan off-design characteristics

The off-design performance of the fan component is modelled based on the fan-characteristic map provided in [18]. The fan in [18] is regarded to have levels of efficiency and pressure ratio similar to what is expected for the GEnx-1B fan. The map is then scaled in a suitable reference point with respect to values of inlet corrected mass flow W_R, pressure rise over inlet pressure (i.e. $\Pi - 1$) and isentropic efficiency η in the cycle design point.

2.2 Model matching

The operating points that together define the thermodynamic cycle of the engine in this study are chosen based on the available data and under what conditions the data has been obtained. The following public sources are utilized:

- Type certificate data sheets from EASA [17] and FAA [15].
- Aircraft engine emission databank (EDB) provided by the International Civil Aviation Organization [19].
- The engine manufacturer [20].
- Efficiency correlations from literature [13].

Based on data extracted from the sources above, the operating points shown in Table 1 were chosen. The table also shows the rating setting used in the different points. In top-of-climb the rating is set by a nominal value for OPR provided in [20]. The nominal net thrust value in max cruise is then assumed to be 1/1.14 of the net thrust in TOC.

In Figure 3 the model matching scheme is illustrated. Dependent variable values are specified as input to the external solver. Residuals are formulated for each dependent variable as the normalized difference between the specified value and the output value from the performance calculation. The Broyden method [12] is then used to evaluate the Jacobian of the system and update the independent variables. This process is iterated until the normalized residuals are smaller than a tolerance value of 1×10^{-5}, upon which the model matching is deemed converged.

2.2.1 Fuel flow

Compressor and turbine efficiencies are among the primary factors that influences the fuel flow. The efficiency correlations previously described, will be used to specify a value taking the most relevant effects into account resulting in an efficiency η_{Grieb}. To satisfy the required fuel flow in $\mathrm{TO_{ISA}}$ given by the EDB data, a common factor δ_η is applied to the component efficiencies. In the model-matching step, δ_η is applied to all compressor and turbine components in the design point (MCR) as an independent variable accordingly:

$$\eta = 1 + (1 - \eta_{Grieb}) \times \delta_\eta. \tag{4}$$

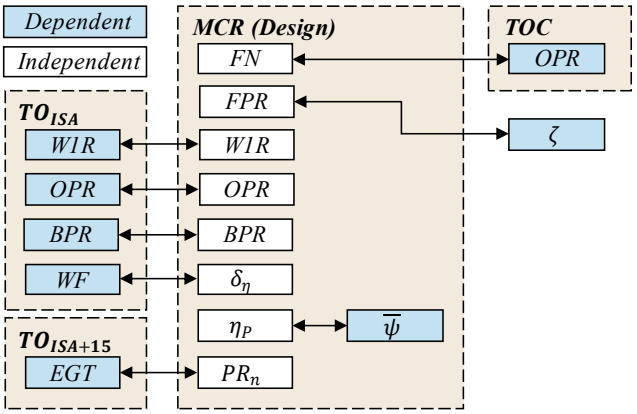

Figure 3: An illustration of the model matching scheme showing the dependent-independent pairs for the external solver.

Table 1: Operating conditions and thrust rating for each point considered in the model matching.

	Operating Condition	Power Setting
Max cruise (MCR)	(35kft, 0.85) ISA	Net thrust specified as fraction of TOC thrust
Top-of-climb (TOC)	(35kft, 0.85) ISA	Set by target OPR
Take-off std. day (TO_{ISA})	SLS, ISA	Net thrust according to ICAO
Take-off hot day (TO_{ISA+15})	SLS, ISA+15	Net thrust according to ICAO

2.2.2 Fan pressure ratio

In order to set the fan pressure ratio in design, the ideal exhaust-jet velocity-ratio (ζ) is added as a dependent variable. This parameter is defined as the ratio of the ideally expanded jet velocity between the bypass and the core nozzle exits.

$$\zeta = \frac{V_{I,18}}{V_{I,8}} \tag{5}$$

For a fixed bypass ratio and specific thrust, the value of ζ that minimizes the required power output from the core for a given operating point can be estimated. Guha [21], found that the jet velocity ratio at this optimum, is approximately equal to the product of the fan and the LPT isentropic efficiencies, i,e.,

$$\zeta \approx \eta_{fan} \times \eta_{LPT}. \tag{6}$$

This condition does however not consider effects of weight and drag on the mission fuel burn, but aims to minimize SFC for the bare engine at a given operating condition. Fulfilling the condition for one operating point will also not guarantee the condition to be fulfilled in the rest of the flight envelope. In addition, the cycle design will in the end be a result of a tradeoff between mission fuel burn and the direct operating cost (DOC). In a study done by General Electric in 1976, the value of ζ at TOC that minimized DOC was found to be approximately 2/3 for a given specific thrust or fan diameter [22]. When further increasing ζ and thereby the power extraction from the core, penalty in weight and maintenance cost due to the need for an additional low-pressure turbine stage outweighed the benefit from a decreased SFC. This result gives an indication that engines in practice are designed with a lower ζ than what is dictated by Eqn. (6).

In order to explore the effects of ζ on other performance and design parameters in the current study, values of ζ at MCR will be sampled from a relatively wide uniform distribution ranging between 0.7 and 0.9. Comparisons will be made with results from samples when ζ is fulfilling the condition in Eqn. (6) at MCR, and when ζ is equal to 2/3 at TOC respectively.

2.2.3 Pressure system power-split

With the OPR, fuel flow, BPR and mass flow specified in TO_{ISA}, the temperature at the HPT inlet can be derived. By knowing the exhaust gas temperature (EGT) one could then obtain the pressure ratio over the HPC and thereby the pressure ratio split between the HPC and the inner part of the fan + booster section (i.e. LPC). This pressure ratio split is from here on measured by the pressure ratio split exponent defined as:

$$PR_n = \frac{ln(\Pi_{LPC})}{ln(\mathrm{OPR})}. \tag{7}$$

From the type certificate datasheet, the redline EGT is provided together with a description of the temperature probes location. For the GEnx, this measurement takes place in the nozzle vanes of the second LPT-stage and amounts to a value of 1338K [17, 15]. Together with assumptions on margins towards this value for the highest rated engine version (GEnx-1B76 according to EDB), the target value for this parameter on a hot-day take-off is obtained. EGT margin for the GEnx engine is estimated based on available data for the CFM56-7B engine where a margin of 55 ΔK to the redline value is reported for a newly manufactured max rated version [23]. Including the EGT in the TO_{ISA+15} point as a dependent variable thus specifies the pressure split between the low- and the high-pressure system.

2.3 Sampling of engine design parameters

The most general form of sampling techniques is the so-called Monte Carlo method in which a *random number generator* produces a uniform sample of *N* points – independently – on the unit interval that are subsequently mapped to a known probability distribution. For weakly non-linear problems it can be beneficial to choose a sample technique with a larger convergence rate compared to the Monte Carlo method in order to reduce the amount of sample points necessary. One example of this is the (Random) Latin Hyper Cube Sampling technique, that was chosen for the purpose of this study. Latin hyper cube sampling differ from the Monte Carlo method in that the unform sample is generated by dividing the unit interval into *N* equally spaced bin. Each bin is then allocated with one sample point, randomly positioned within the boundaries of the bin. The distribution of the sample points along the unit interval is randomized between the input parameters in order to allocate the

solution space sufficiently and minimize the risk of correlations between them.

Uncertainties will be considered for the dependent variable values as well as the remaining design and off-design parameters of interest. Except for the ideal jet velocity ratio ζ at MCR, normal distributions will be assumed with estimated standard deviations and mean values. To exclude unphysical solutions all the normal distributions are truncated at the $\pm 4\sigma$ limit.

Three different samples will be generated, that are identical apart from how the jet velocity is treated. For the ideal jet velocity ratio in sample nr 1, a simple interval defining a uniform distribution will be used. This is done since the precise value is considered likely to be anywhere between 0.70 to 0.9 depending on choices regarding trade factors that were made during the design process, such as production-/development cost vs energy efficiency. As described earlier, ζ will also be set to a fixed value of 2/3 at TOC (sample 2) and alternatively specified in accordance with Eqn. (6) at MCR (sample 3).

For some of the data that originates from the SLS-rig measurements, typical values for measurement uncertainty as provided by Smith [24] have been applied. For a complete list of variables and corresponding probability distributions see Appendix A.

2.3.1 Uncertainty estimation of efficiency

To evaluate the uncertainty of the efficiency – loading relationship as given by Eqn. (2), the approach for each component has been to establish a higher and a lower efficiency trend curve, based on the source data. These two curves are then assumed to represent the prediction band of two standard deviations, $f_{+2\sigma}$ and $f_{-2\sigma}$, from a mean f_{μ}, assuming a normal distribution. A sampled trend line is then given by the expression:

$$\eta^*_{pol} = f_{\mu}(\overline{\psi}) + X f_{\sigma}(\overline{\psi}), \tag{8}$$

where X is sampled from a normalized gaussian distribution – independently for each compressor and turbine component – and where the two functions f_{μ} and f_{σ} are given accordingly:

$$f_{\mu}(\overline{\psi}) = \frac{f_{+2\sigma}(\overline{\psi}) + f_{-2\sigma}(\overline{\psi})}{2}. \tag{9}$$

$$f_{\sigma}(\overline{\psi}) = \frac{f_{+2\sigma}(\overline{\psi}) - f_{-2\sigma}(\overline{\psi})}{4}. \tag{10}$$

The distributions of X are furthermore truncated at the $\pm 4\sigma$ limit to prevent unphysical solutions. In Figure 4, the $\pm 2\sigma$ and the resulting μ trend curves are plotted together with the source data for each component.

3. RESULTS AND DISCUSSION

The design and performance parameters obtained at MCR are listed in Table 2. The sample size for the case with a uniform distribution of jet velocity-ratio ζ, (sample 1), amounted to 1189. Likewise, a total of 1187 and 1183 runs were sampled for the case with a constant ζ at TOC (sample 2) and with Eqn. (6) fulfilled at MCR (sample 3), respectively. A comparison of the resulting design and performance parameters of interest at MCR are listed in Table 2 in terms of the median, the 2.5 percentile and the 97.5 percentile. Only small differences between the three samples can be noted for all parameters except FPR. Sample 2 lies in the lower part of the FPR range and sample 3 in the upper. The 2.5 to 97.5 inter-percentile range of FPR for sample 2 and 3 amounts to 0.030 and 0.037 points respectively.

Figure 5 shows the marginal plots of polytropic efficiency and loading for each component at MCR, sampled for the different jet velocity-ratio assumptions. One can observe that the significant variation in FPR and consequently LPT-average stage-loading does not seem to effect the polytropic efficiency for the respective component. This can be attributed to the weak influence the loading has on the normalized efficiency in the input efficiency correlations shown in Figure 4.

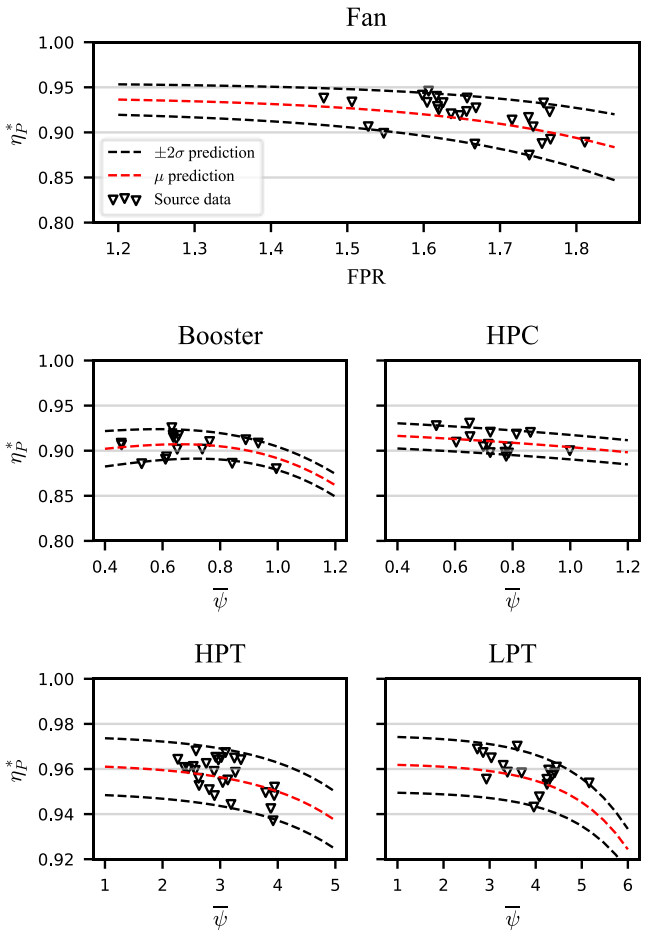

Figure 4: Normalized efficiency correlated against loading based on data reproduced from [13]. Operating point – MCR. Trendlines representing the mean and prediction bands of two standard deviations are shown as well.

The large spread in fan pressure ratio and LPT stage loading indicates that the performance of the low-pressure system is difficult to predict when relying solely on publicly available information. As expected, a narrower range in both metrics is obtained when fixing the jet velocity-ratio, highlighting the need to introduce additional information during the matching procedure. This information can be retrieved from correlations on direct operation cost, fuel burn or engine conceptual design. In the present work we introduced two examples to highlight the importance of energy transfer in the low-pressure system performance metrics. The polytropic efficiencies of the booster and the HPC have a stronger dependency on their individual loading compared to the other components, which can be traced back to the trends for the normalized polytropic efficiencies in Figure 4.

As previously noted, a higher LPT average stage loading seems to correlate well with an increased FPR as one might expect. For the high pressure components and the booster, the distribution of average stage loading is far more independent of the FPR, which goes back to the reasoning behind the model-matching scheme explained in section 2.2.3; assuming that OPR, BPR, mass flow and fuel flow in the MCR point are primarily depending on the provided data for the corresponding parameters in TO_{ISA}, the power extraction from the HPT will primarily depend on the given EGT value ($i.e.T_{4.6}$) and the level of chargeable cooling flow extracted for the LPT. Possible effects due to variations in FPR will hence be overshadowed by the first order effects of variations in OPR, BPR, mass flow and fuel flow in TO_{ISA}.

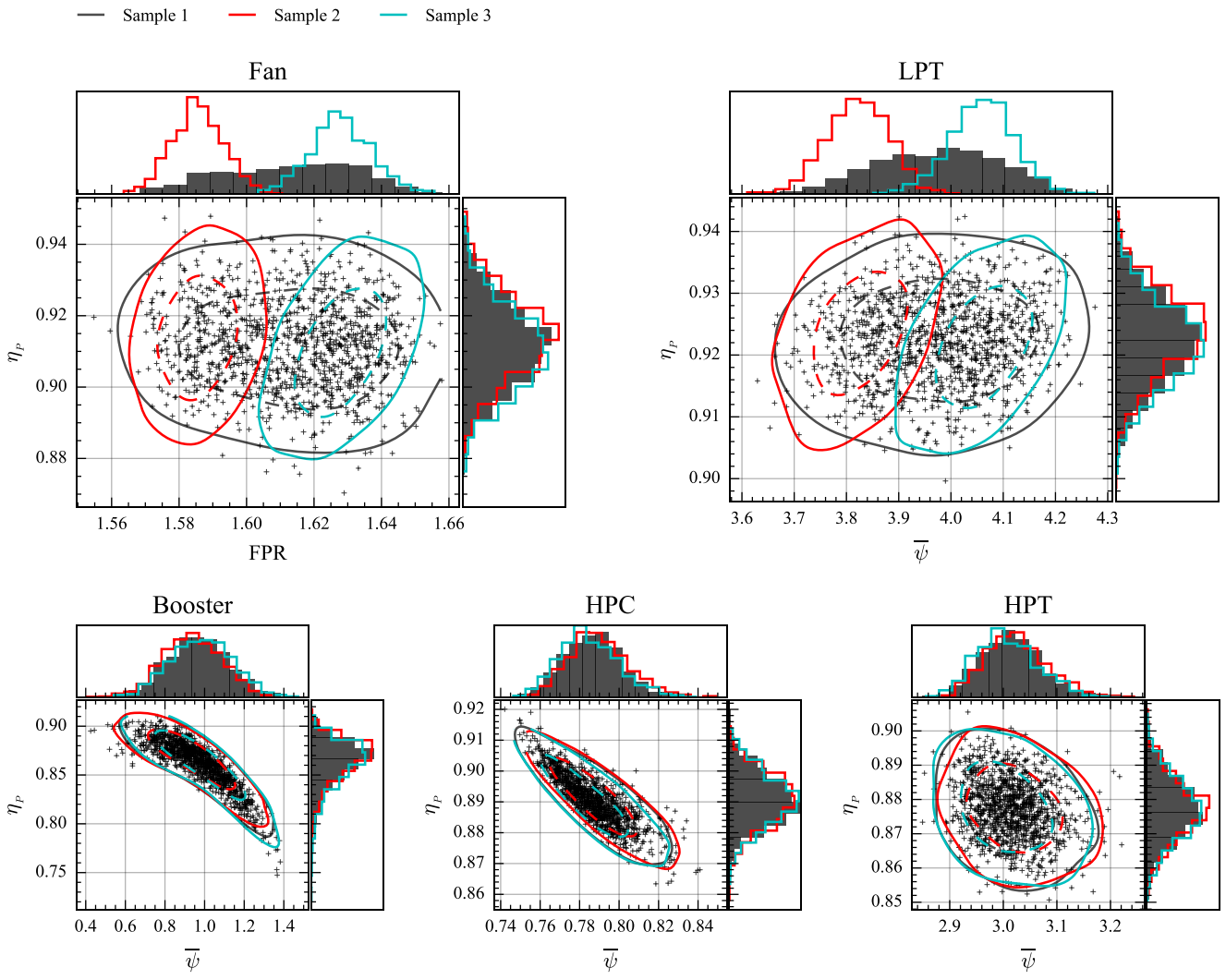

Figure 5: Marginal plots of polytropic efficiency and loading for each component at MCR. Contour lines represent constant probability density for each sample, where solid lines enclose 95% of all individuals and dashed lines 60%. Sample nr 1 is furthermore visualized as a scatter together with the contour

Based on the average corrected mass flow at the inlet to the fan and the area of the fan annulus, the Mach number at the face of the fan is estimated (M_{2A}) at MCR. From the comparison between the distributions of M_{2A} of the three samplings shown in Figure 6, no apparent dependency on ζ can be observed other than a very slight tendency towards lower values for sample 2. Still, the spread in M_{2A} at MCR is substantial and requires further investigation. One of the primary causes for the spread is evidently due to the uncertainty of the provided inlet mass flow at TO_{ISA} [20]. This behavior is illustrated in Figure 7 with the marginal plot for fan face Mach number in MCR and the TO mass flow at ISA conditions.

Table 2: Design & performance parameters at MCR for the GEnx-1B model. The table shows the data sampled for three assumptions on jet velocity-ratio, and is provided for the median, the 2.5 percentile and the 97.5 percentile.

	Sample 1 ζ uniformly distr. at MCR			**Sample 2** $\zeta = 2/3$ at TOC			**Sample 3** ζ according to Eqn. (6) at MCR		
Sample size:	1189			1187			1183		
Percentile:	**50.0**	**2.5**	**97.5**	**50.0**	**2.5**	**97.5**	**50.0**	**2.5**	**97.5**
M_{2A}	0.687	0.672	0.702	0.685	0.670	0.700	0.688	0.673	0.703
FPR	1.615	1.574	1.646	1.585	1.571	1.601	1.628	1.610	1.647
OPR	49.21	48.75	49.67	49.19	48.69	49.64	49.22	48.73	49.68
$T_{4.1}$	1582	1564	1605	1588	1572	1609	1578	1561	1598
PR_n	0.245	0.203	0.273	0.237	0.198	0.265	0.249	0.210	0.276
BPR	8.675	8.562	8.791	8.698	8.591	8.808	8.663	8.551	8.773
$\hat{F}_N$ [m/s]	125.8	122.9	128.7	126.9	124.5	129.3	125.2	122.8	127.6
SFC [mg/Ns]	15.47	15.27	15.67	15.45	15.27	15.65	15.48	15.28	15.67
$\eta_{P,FAN}$	0.912	0.889	0.935	0.914	0.891	0.938	0.910	0.887	0.935
$\eta_{P,Booster}$	0.867	0.804	0.894	0.869	0.815	0.898	0.865	0.791	0.896
$\eta_{P,HPC}$	0.890	0.875	0.907	0.891	0.874	0.906	0.891	0.874	0.908
$\eta_{P,HPT}$	0.877	0.859	0.894	0.877	0.860	0.894	0.877	0.860	0.895
$\eta_{P,LPT}$	0.922	0.908	0.936	0.924	0.910	0.936	0.922	0.908	0.934

Despite a large variation in jet velocity-ratio – and consequently FPR – the resulting spread in SFC at MCR is comparably small. The 2.5 - 97.5 inter-percentile range of SFC at MCR amounts to around 0.39 mg/Ns, as provided in Table 2, which corresponds to about 2.5 % of the median value. The reason for this is that the fuel flow and thrust are given in the standard day take-off operating point, albeit with uncertainty. The SFC in the same point is thereby implicitly given already. Possible differences between the resulting distribution of SFC in TO_{ISA} and MCR could then be explained by input uncertainties influencing the rating at TOC and MCR i.e. the OPR at TOC, and the ratio of net thrust at TOC to MCR. Other effects of importance are those related to changes of engine component off-design characteristics. In this regard, the off-design characteristics of the fan efficiency with respect to the flow capacity and the bypass nozzle pressure ratio with respect to the discharge coefficient, are believed to be of high importance. It is therefore important to emphasize that any relative variations in these relationships have not been included in the present study. With this in mind, comparing the SFC value at MCR and TO_{ISA} shows a high level of correlation for all three samples, as can be seen in Figure 8.

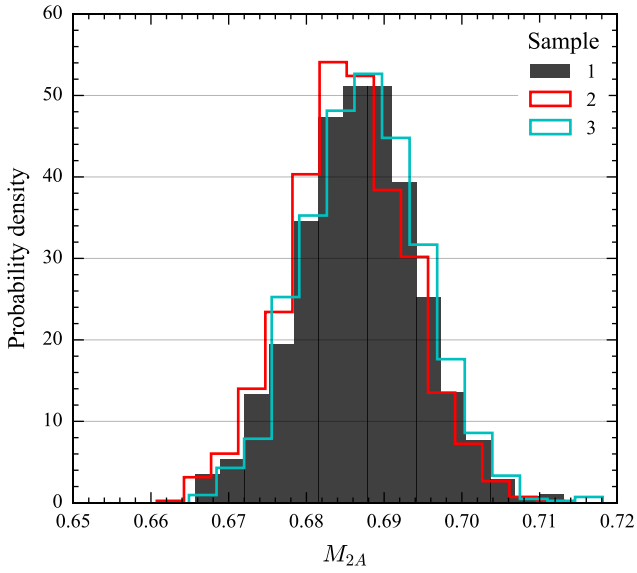

Figure 6: Histograms of the distribution of Mach number at the fan-face for each sampling at MCR.

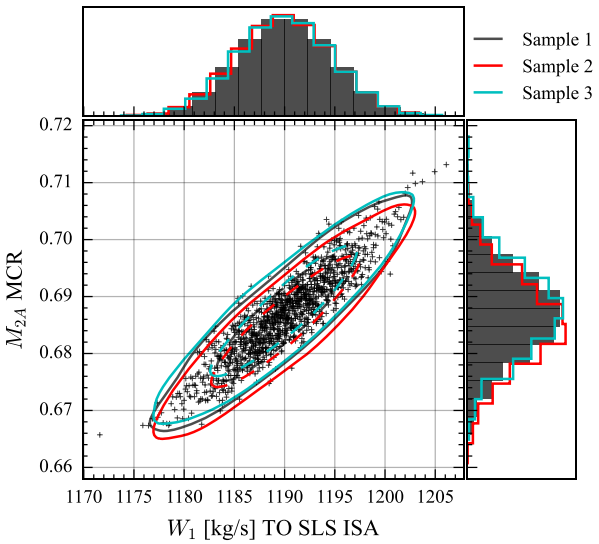

Figure 7: Marginal plot of Mach number at the fan-face at MCR plotted against inlet mass flow in TO_{ISA}. Contour lines and scatter points defined in the same way as for Figure 5.

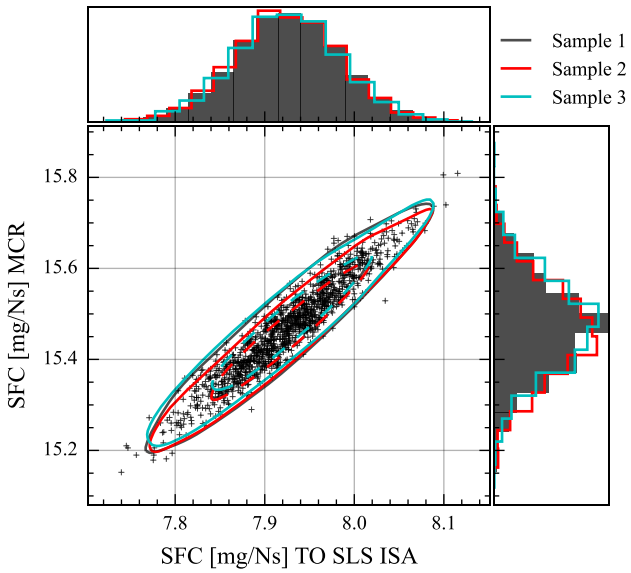

Figure 8: Marginal plot of SFC at MCR and TO_{ISA}. Contour lines and scatter points are defined in the same way as for Figure 5.

4. CONCLUSION

In the present work, Latin Hypercube Sampling was used to estimate the level of uncertainty in the results when matching a cycle performance model to public data on the GEnx-1B commercial aircraft engine.

The results show that the fuel burn performance can be predicted with some degree of confidence. However, it also indicates that a larger degree of uncertainty is expected when predicting the performance of the low-pressure system. The SFC range in the spread is 2.5% of the median, whereas the corresponding range for the FPR is 4.5%. When a constant value for the jet-velocity-ratio was provided at TOC the range in fan pressure ratio in relation to the median dropped to 1.89%, whereas the SFC range remained constant. The reason for this behavior is that there is no first-order effects on the MCR SFC from a variation in FPR in this particular case since the SFC at TO_{ISA} is fixed from the input data provided by the engine emission database. The absence of any significant trend between the resulting polytropic efficiency and the fan pressure ratio is a result of a large spread in the empirical input model between the FPR and the unmatched polytropic efficiency, as well as a weak influence on the SFC at take-off from a change in FPR.

The range in the fan-face Mach number spread in relation to the mean is about 4.4%. It is believed that the uncertainty in this parameter was primarily influenced by variations in the inlet mass flow in the take-off sea-level-static point. The mass flow is provided for take-off by the manufacturer in [20], but little information is provided with respect to the operating conditions in which it was measured.

To conclude, the present study highlights the importance of statistic-based methods as a support tool for the inverse design procedure. The results obtained quantify the limitations of conventional thermodynamic matching, when relying solely on publicly available data. Such matching procedure, although valid and important, requires the support of studies on conceptual design, cost and fuel burn, to be able to estimate the low-pressure system performance metrics with a high degree of certainty.

ACKNOWLEDGEMENTS

This research work was funded by the Swedish National Aviation Engineering Research Program, NFFP, supported by Swedish Armed Forces, the Swedish Defense Material Administration and the Swedish Governmental Agency for Innovation Systems, VINNOVA.

REFERENCES

[1] M. Verbist, W. Visser, J. van Buijtenen and R. Duivis, "Gas path analysis on KLM in-flight engine data," *Turbo Expo: Power for Land, Sea, and Air*, 2011.

[2] F. S. Mastropierro, J. Sebastiampillai, F. Jacob and A. Rolt, "Modeling Geared Turbofan and Open Rotor Engine Performance for Year-2050 Long-Range and," *ASME. J. Eng. Gas Turbines Power.*, p. 142, April 2020.

[3] D. Mavris, N. Macsotai and B. Roth, "A Method for Probabilistic Sensitivity Analysis of Commercial Aircraft Engines," *AIAA*, 1999.

[4] D. Mavris, N. Macsotai and B. Roth, "A Probabilistic Design Methodology For Commercial Aircraft Engine Cycle Selection," *SAE*, 1998.

[5] K. G. Kyprianidis, V. Sethi, S. O. T. Ogaji, P. Pilidis, R. Singh and A. I. Kalfas, "Uncertainty in gas turbine thermo-fluid modelling and its impact on performance calculations and emissions predictions at aircraft system level," *J. Aerospace Engineering*, vol. 226, 2011.

[6] T. Gronstedt, "Development of methods for analysis and optimization of complex jet engine systems," *Doktorsavhandlingar vid Chalmers Tekniska Hogskola*, nr 1595, pp. 1-93, 2000.

[7] T. Grönstedt, M. Irannezhad, X. Lei, O. Thulin and A. Lundbladh, "First and Second Law Analysis of Future Aircraft Engines," *J. Eng. Gas Turbines Power*, vol. 136, nr 3, p. 031202, 2014.

[8] O. Thulin, O. Petit, C. Xisto, X. Zhao and T. Grönstedt, "First and Second Law Analysis of Radical Intercooling Concepts," *J. Eng. Gas Turbines and Power*, vol. 140, nr 8, p. 081201, 2017.

[9] C. Xisto, O. Petit, T. Grönstedt and A. Lundbladh, "Assessment of CO2 and NOx Emissions in Intercooled Pulsed Detonation Turbofan Engines," *J. Eng. Gas Turbines Power*, vol. 141, nr 1, p. 011016, 2019.

[10] L. Xu and T. Grönstedt, "Design and Analysis of an Intercooled Turbofan," *J. Eng. Gas Turbines Power*, vol. 132, nr 11, p. 114503, 2010.

[11] X. Zhao, O. Thulin and T. Grönstedt, "First and Second Law Analysis of Intercooled Turbofan Engine," *J. Eng. Gas Turbines Power*, vol. 138, nr 2, p. 021202, 2015.

[12] J. S. Gray, J. T. Hwang, J. R. Martins, K. T. Moore and B. A. Naylor, ”OpenMDAO: an open-source framework for multidisciplinary design, analysis, and optimization,” *Structural and Multidisciplinary Optimization,* vol. 59, nr 4, 2019.

[13] H. Grieb, Projektierung von Turboflugtriebwerken, 1st red., Basel: Springer Basel AG, 2004.

[14] S. Samuelsson, T. Gronstedt and K. G. Kyprianidis, ”Consistent conceptual design and performance modeling of aero engines,” *Proceedings of the ASME Turbo Expo,* vol. 3, nr March, 2015.

[15] FAA, "Type-certificate data sheet E00078NE," 20 May 2020. [Online]. Available: https://rgl.faa.gov/Regulatory_and_Guidance_Library/rgMakeModel.nsf/0/1f7cee7136ca6db48625856f0069f05a/$FILE/E00078NE_Rev16.pdf. [Accessed 19 Oktober 2020].

[16] P. R. N. Childs, ”Gas Turbine Engine Internal and Secondary Flow System,” 2018. [Online]. Available: https://jet-engine-lab.technion.ac.il/files/2018/11/A2-2018-Jet-Engine-Conference-Bruno-Aguilar-Honeywell.pdf.

[17] EASA, "Type-certificate data sheet No. IM.E.102," 13 December 2019. [Online]. Available: https://www.easa.europa.eu/sites/default/files/dfu/TCDS%20IM%20E%20102_issue10_20191213.pdf. [Accessed 19 Oktober 2020].

[18] C. Freeman, ”Method for the Prediction of Supersonic Compressor Blade Performance,” *Journal of Propulsion,* vol. 8, nr 1, 1992.

[19] ICAO, "Aircraft Engine Emissions Databank v26B," 20 September 2019. [Online]. Available: https://www.easa.europa.eu/sites/default/files/dfu/edb-emissions-databank v26B-NewFormat %28web%29.xlsx. [Accessed 19 Oktober 2020].

[20] GE Aviation, "Datasheet GEnx," [Online]. Available: https://www.geaviation.com/sites/default/files/datasheet-genx.pdf. [Accessed 19 Oktober 2020].

[21] A. Guha, ”Optimum Fan Pressure Ratio for Bypass Engines with Separate or Mixed Exhaust Streams,” *Journal of Propulsion and Power,* vol. 17, nr 5, 2001.

[22] R. E. Neitzel, R. Hirschkron and R. P. Johnston, ”Study of Turbofan Engines Designed for Low Energy Consumption,” Cincinnati, 1976.

[23] S. Ackert, "Engine maintenance management," 15 May 2015. [Online]. Available: http://www.aircraftmonitor.com/uploads/1/5/9/9/15993320/engine_mx_management_madrid_may-12_2015.pdf. [Accessed 19 Oktober 2020].

[24] R. E. Smith, ”Marrying Airframes and Engines in Ground Test Facilities: An Evolutionary Revolution,” *Journal of Aircraft,* vol. 33, nr 4, 1996.

Appendix A

Data values and distributions for inputs to the model matching by operating point. The specified normal distribution for an independent random variable is abbreviated $N(\mu, \sigma)$.

MCR:

	Nominal value	Source	Distribution
P_{2A}/P_1	0.998	-	$N(0.998, 0.00010)$
HPX [kW]	330.0	[17]	$N(330.0, 15.0)$
$C_{V,18}$	0.995	-	$N(0.995, 0.00025)$
$C_{V,8}$	0.977	-	$N(0.977, 0.00115)$
P_{18}/P_{13}	0.99	-	$N(0.990, 0.00050)$
P_8/P_5	0.985	-	$N(0.985, 0.00075)$
$P_{2.5}/P_{2.3}$	0.988	-	$N(0.988, 0.00060)$
η_P^*	See 2.3.1	[13]	See 2.3.1

TO_{ISA}:

	Nominal value	Source	Distribution
F_N [kN]	341.2	[19]	$N(341.2, 1.7)$
OPR	46.4	[19]	$N(46.6, 0.14)$
BPR	8.7	[19]	$N(8.7, 0.05)$
W_f [kg/s]	2.704	[19]	$N(2.704, 0.002)$
W_1 [kg/s]	1190	[20]	$N(1190.0, 4.8)$
P_{2A}/P_1	1.0	[19]	Fixed
HPX [kW]	0.0	[19]	Fixed
Ω_L [rpm]	2560	[15]	Fixed
Ω_H [rpm]	11377	[15]	Fixed

TO_{ISA+15}:

	Nominal value	Source	Distribution
F_N [kN]	349.2	[19]	$N(349.2, 1.8)$
$T_{4.6}$[K]	1283	[17]	$N(1283, 2.6)$
P_{2A}/P_1	1.0	[19]	Fixed
HPX [kW]	330.0	[17]	*Same as MCR*

TOC:

	Nominal value	Source	Distribution
OPR	55.4	[20]	$N(55.4, 0.17)$
P_{2A}/P_1	0.998	-	*Same as MCR*
HPX [kW]	330.0	[17]	*Same as MCR*

General:

	Nominal value	Source	Distribution
$F_{N,TOC}/F_{N,MCR}$	1.14	[13]	$N(1.14, 0.005)$
$W_{B,3.0}$	0.22	-	$N(0.22, 0.011)$
$W_{B,2.5}$	0.05	-	$N(0.05, 0.0025)$
ζ	See 2.3	-	See 2.3